Laser and Particle Beams (1995), *vol.* 13, *no.* 4, *pp.* 511–524
Printed in the United States of America

Measurements of thermal transport in plasmas produced by picosecond laser pulses

By L.A. GIZZI, A.J. MACKINNON, D. RILEY, S.M. VIANA, AND O. WILLI

The Blackett Laboratory, Imperial College of Science, Technology and Medicine, Prince Consort Road, London, SW7 2BZ, England

(Received 5 April 1995; revised 11 June 1995; accepted 5 July 1995)

In this paper we present measurements of energy transport in hot, high-density plasmas produced by picosecond laser interaction with solid targets. The propagation of the ablative heat wave was studied by using X-ray–ultraviolet (XUV) spectroscopy with picosecond temporal resolution. Measurements show that for laser intensities on target above 10^{16} W/cm^2, strong inhibition of heat flux toward the cold target occurs. A detailed modelling of the experimental data is presented in which heat transport and absorption processes are taken into account self-consistently. Finally the role played by lateral transport and self-induced magnetic fields in our experiment is also discussed.

1. Introduction

The production of hot, high-density plasmas is of great significance to basic atomic physics and X-ray laser research (Rosen 1990; Murnane & Kapteyn 1991). Such plasmas can be generated when a high-power, short-pulse laser light is focused onto solid targets. Early during the laser heating process, a supersonic, nonlinear heat wave is launched into the target. Hydrodynamic expansion soon takes place with consequent shock formation. Laser light propagates in the inhomogeneous underdense plasma where most of the energy is absorbed via collisional as well as collisionless processes. The shock wave separates from the heat wave, now subsonic, giving rise to the so-called ablative heat-wave regime (Meyer-Ter-Vehn 1984). According to this picture, the hydrodynamic behavior of the overdense plasma region beyond the absorption region is therefore strictly related to energy absorption and thermal transport phenomena.

The modelling of heat propagation in the simulation of laser–plasma interaction experiments is presently being performed mainly by using the classical flux-limited Spitzer–Harm (SH) thermal conductivity (Spitzer & Harm 1953). On the other hand, detailed 2D Fokker–Planck (FP) codes have already been successfully applied (Rickard *et al.* 1989) to the interaction of high-intensity laser light with hot dense plasmas. Nevertheless, the implementation of numerical codes for the simulation of laser–plasma interaction experiments with FP routines is presently still cumbersome due to the large amount of computer-time needed. A comparison of the results obtained using the two different approaches to describe thermal transport in simple physical systems can provide valuable information on the constraints, as well as the range of validity of the classical flux limited description.

Since the heat flux cannot be measured directly, physical quantities depending on thermal transport are taken into account (Kruer 1988). In fact, the mass ablation rate can be evaluated (Key *et al.* 1983) from burn-through measurements in multilayered targets by studying the temporal evolution of X-ray emission whose spectral components are characteristic of each layer of the target.

 0263-0346/95 $11.00 + .10

An intense experimental activity has been devoted to the investigation of thermal transport in laser-produced plasmas in planar and spherical geometry in a nanosecond regime (Dahmani & Kerdja 1991, and references therein). The temporal dependence of the mass ablation rate has also been studied in UV-laser-irradiated spherical targets (Jaanimagi 1986). In that investigation the authors pointed out that time-dependent effects occurring during the laser pulse can significantly complicate the dynamics of thermal transport mechanisms.

In this paper we report on measurements of electron transport in hot, high-density plasmas produced by irradiation of solid targets with picosecond laser pulses at intensities on target up to few times 10^{16} W/cm^2. Sub-keV spectroscopy with picosecond temporal resolution was used to investigate the propagation of the ablative heat wave in layered targets. The results of these measurements will be discussed in view of detailed absorption measurements performed (Riley *et al.* 1993) under the same experimental conditions. A detailed modelling of the experimental data will be presented in which thermal transport and absorption processes are taken into account self-consistently. The interplay between the two processes shows that lateral transport may occur in the underdense plasma, where nonlinear collisional absorption and resonance absorption account for the transfer of laser energy to the plasma. A strong reduction of the mass ablation rate observed in the high-laser intensity limit will be discussed in view of experimental observations that suggest that a strong self-generated magnetic field may take place during the interaction.

2. Experimental setup

The 12-ps, 0.268-μm pulse of the SPRITE laser at the Central Laser Facility of the Rutherford Laboratory (DRAL) was focused onto solid targets at irradiances up to 3×10^{16} W/cm^2. Mass ablation rate measurements were performed using targets consisting of a 10-μm-thick Mylar substrate coated with 2000 Å Al and overcoated with a thin (1000 Å) low-Z plastic ablator (CH). The particular choice of material and thickness of each layer of the target will be discussed below. The primary diagnostic was a time-resolving XUV spectrometer consisting of a grazing incidence flat field grating (Nakano *et al.* 1984) coupled to an X-ray streak-camera. Mass ablation rates were inferred from the history of line emission intensity originating from the target signature layers as the heat front propagated in the target. The spectral range of the spectrometer was chosen to detect characteristic line emission from each one of the three layers.

Line emission at 33.74 Å from H-like Carbon (C-Lyα) in the C–H layer, at XX Å from Li-like Aluminum (Li $1s^2 2p$-$1s^2 4d$) in the middle Al layer and both H-like Carbon (C-Lyα) and at 19.97 Å H-like Oxygen (O-Lyα) from the Mylar substrate were detected in the same spectra. The streak-camera used to resolve temporally the spectrum was fitted with a KBr photocathode, which enabled a temporal resolution as high as $\approx$2 ps to be achieved.

The angular dependence of absorption of S and P polarized light was studied using a 10-cm diameter Ulbricht sphere (Godwin *et al.* 1977), which collected the light scattered by a thick Al target placed at the center of the sphere. A detailed description of the whole experimental setup used for absorption measurements can be found elsewhere (Gizzi 1994).

3. Experimental results

3.1. *Spectroscopic measurement of mass ablation rate*

The temporal evolution of the above specified Oxygen, Carbon, and Aluminum spectroscopic lines obtained at an irradiance of 3×10^{16} W/cm^2 is shown in figure 1. The first peak of the C-Lyα emission arises from the first C–H layer. As the temperature in this

region increases, Carbon atoms soon become fully stripped and C-Lyα emission intensity falls. Then the heat front propagates into the Al layer giving rise to Li-like Al emission. Finally C-Lyα emission takes place again when the inner Mylar substrate is reached by the ablative heat wave. Due to the nominal target composition and configuration, emission from Oxygen ions should resemble the second peak of carbon emission. However, though such an emission lasts longer than the Al emission from the middle layer, it starts almost simultaneously. This can be explained by taking into account Oxygen impurities in the Aluminum layer due to the presence of Al oxide (Al_2O_3). In fact, strong Oxygen emission was systematically detected when solid "pure" Aluminum targets were irradiated in similar experimental conditions.

Assuming that the history of the line emission shown in figure 1 mainly depends upon the heat propagation and that atomic processes are fast compared to the typical time-scale of mechanisms, one can determine the mass ablation rate. Considering the density and the thickness of the ablated Al layer and the peak-to-peak separation in the history of C-Lyα of 22 ps $\pm$ 2 ps one finds a mass ablation rate of 2.4×10^6 g cm^{-2} s^{-1} $\pm$ 10%. A similar procedure used for a lower incident intensity of 4.3×10^{15} W/cm^2 gives a mass ablation rate of 3.4×10^6 g cm^{-2} s^{-1} $\pm$ 10%. Before proceeding with the analysis of these results it is necessary to discuss the validity of the simple assumptions made above.

3.2. *Transient effects in line emission processes*

The main feature of figure 1 is the temporal evolution of C-Lyα line, which is characterized by two maxima separated by 22 ps $\pm$ 2 ps. We observe that for this radiation to be a good diagnostic for measurements of heat propagation, atomic physics processes must be fast compared to hydrodynamic ones. In the experimental investigation on mass ablation rate published so far, nanosecond laser pulses were mainly considered and the ablation rate was typically inferred from the temporal evolution of H-like Al or H-like Si lines. It can be shown that, at the densities and temperatures typical of laser-produced plasmas in the nanosecond regime, ionization times ranging from several tens to hundred picoseconds can be expected. Therefore, the accuracy of ablation rate measurements from time resolved X-ray spectroscopy of highly ionized, medium Z plasmas, could be affected by

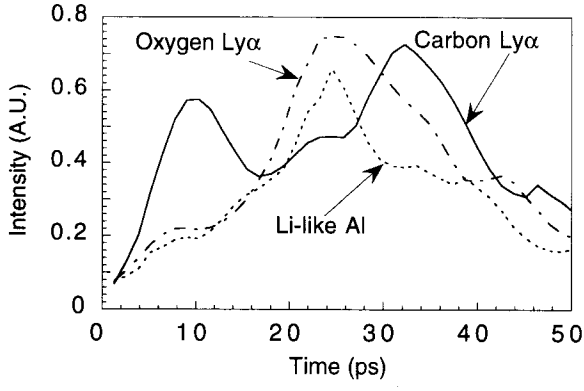

FIGURE 1. Temporal evolution XUV line emission from laser irradiation of a C-H-Al-Mylar target at an irradiance of 3×10^{16} W/cm^2. Line emission from H-like Carbon (C-Lyα), from the C-H layer, Li-like Aluminum (Li $1s^2 2p$-$1s^2 4d$) from the middle Al layer and both H-like Carbon (C-Lyα) and H-like Oxygen (O-Lyα) were detected simultaneously.

time-dependent atomic physics effects. Regardless of the particular temporal regime under investigation, time-dependent effects on mass ablation rate measurements carried out using X-ray emission have to be carefully examined. On the other hand, one may regard transient atomic physics effects as giving rise to constraints on the particular atomic transition process to be selected for the particular temporal scale under investigation.

Concerning the experiment described here and considering that we are dealing with emission from low-Z elements (Carbon and Oxygen) or Li-like Al, we expect the condition for a steady-state model to be fulfilled. In fact, a quantitative analysis of the ionization times relevant to our experimental configuration was carried out by calculating the rates of the most important ionization processes, namely collisional, three-body, and radiative ionization. It was found that the relaxation time for ionization from He-like to H-like Carbon at electron temperatures up to 1 keV and at the critical density for 0.25-μm laser light, that is, 1.5×10^{22} cm^{-3}, was comparable to, or less than 1 ps. Similar values were found for the case of ionization from Be-like to Li-like Aluminum. A slightly longer relaxation time of 2 ps was found for the ionization from He-like to H-like Oxygen.

Another mechanism that can influence the response of atomic physics processes to the hydrodynamic evolution of the plasma is the radiative spontaneous emission. The time-scale of radiative spontaneous emission for the three bound–bound transitions considered above was calculated by using the available oscillator strengths (Martin & Wiese 1983). The decay times of C-Lyα, O-Lyα, and Li $1s^2 2p$-$1s^2 4d$ line emission were found to be 1.6 ps, 0.5 ps, and 3 ps, respectively. In view of these results and taking into account the experimental data considered above, we can conclude that, although transient effects can affect the observed history of the line emission, their contribution to the experimental uncertainty is expected to be small. Consequently, the main features of the X-ray emission processes taken into account in this study are expected to be mainly related to the hydrodynamic evolution of the plasma.

3.3. *Absorption measurements*

A better understanding of the processes analyzed so far can be achieved by linking the results of thermal transport measurements to the measurements of absorption of laser energy. A detailed analysis of these measurements has been presented elsewhere (Riley *et al.* 1993). In that work it was found that the measured absorption of S- and P-polarized light was consistent with a one-dimensional (1-D) hydrodynamic modelling assuming a classical description of resonance and collisional absorption. The results concerning thermal transport presented in this work suggest an alternative approach to the interpretation of absorption measurements as described below.

Solid Al targets were irradiated at an average intensity 5×10^{16} W/cm^2 in a $\approx$20-μm diameter focal spot. We studied the dependence of the absorption coefficient upon the angle of incidence and the polarization of the laser light. Figure 2 shows the dependence of the fractional scattering of laser light upon the angle of incidence in the case of S-polarized light. A maximum absorption of approximately 30% occurs at normal incidence. The absorption decreases as the angle of incidence increases and almost 100% of the laser light is scattered by the target for angles of incidence greater than 40 degrees.

According to the theory of propagation of S-polarized electromagnetic (EM) waves in inhomogeneous plasmas in the conditions under investigation here, inverse bremsstrahlung absorption is expected to be the primary energy transfer mechanism. The absorption efficiency at a given angle of incidence primarily depends upon two plasma parameters, namely the electron density scale length and the electron temperature of the subcritical density region. A relatively precise measurement of the density scale length was obtained by absorp-

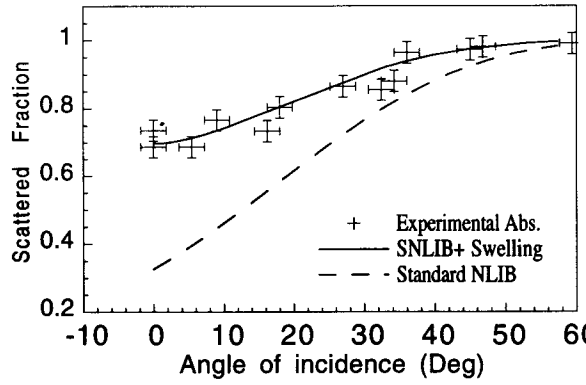

FIGURE 2. Fractional scattering of laser energy incident on a solid Al target at an intensity of 5×10^{16} W/cm^2 as a function of the angle of incidence and for *S*-polarized light. Both diffused scattering and collimated back-scattering were collected and measured. The solid and dashed lines show the result of the calculation (see text).

tion measurements as a function of the angle of incidence for *P*-polarized light. In fact, in the case of *P*-polarized EM waves incident onto an inhomogeneous plasma, a maximum conversion of laser energy into longitudinal electron plasma waves occurs for an angle of incidence θ_{max} given by the relation $\sin(\theta_{max}) = (\frac{1}{2}kL)^{1/3}$.

The minimum scattering of *P*-polarized light and therefore, the maximum absorption, was found to occur at an angle of incidence $\theta_{max} \cong 10 \pm 1$ deg. At this angle, approximately 45% of the incident laser energy is transferred to the plasma. In other words, the occurrence of resonance absorption accounts for a maximum extra absorption of 20% of the incident laser energy. According to the theory (Kruer 1988), resonance absorption alone can account for an absorption of as much as 50% of the incident energy. Therefore, in our experimental conditions, this absorption process is much less effective than predicted by the theory. However, it has been shown that (Perry *et al.* 1989), in the case of interaction of 20–120 ps, 1-μm laser pulses focused on solid target, the occurrence of either the parametric decay instability or ion turbulence can strongly inhibit resonance absorption in favor of an enhanced collisional absorption process. In our experimental conditions, where shorter wavelength and pulselength were used, this effect is not so dramatic, probably due to the shorter density scale length and therefore to the higher threshold intensity for the activation of the parametric instability. Therefore, in our experimental conditions, resonance absorption still accounts for an important fraction of the absorbed energy, although this mechanism is not so efficient as predicted by the theory.

According to the expression given above, the measured angle of maximum resonance absorption gives a density scale length in the subcritical region of 4.3 ± 1.2 μm. It is instructive to compare this result with a simple estimate of the density scale length obtained by considering a self-similar expansion of a 1-D isothermal plasma (Kruer 1988). According to this model, the density scale length increases linearly with the time t, and is simply given by $L = v_s t$, where v_s is the sound velocity. In the case of a fully ionized Al plasma at an electron temperature of 2 keV, the speed of sound is 0.35 μm/ps. The particular choice of the electron temperature considered here will be discussed in detail below. According to these assumptions, after approximately 10 ps from the beginning of the interaction the density scale length is predicted to be 3.5 μm, which is consistent with the measured value reported above. A more accurate modelling of the temporal evolution of the density scale

length at the critical density was carried out with the hydro-code MEDUSA (Christiansen 1974).

4. Hydrodynamic simulations

4.1. *Longitudinal density scale length*

The temporal dependence of the electron density profile of the plasma was calculated by MEDUSA for the experimental conditions considered above. A full description of the results of numerical hydrodynamic simulations is reported elsewhere (Gizzi 1994). The portion of the density profile, for densities just below the critical density, was fitted using a linear function and the corresponding scale length was calculated according to its definition, $L = n_e/(\partial n_e/\partial x)$. The result is shown in figure 3 as a function of the time relative to the peak of the pulse.

According to this result, two regimes of expansion can be identified, one before and one after the peak of the laser pulse, respectively. In the first stage of expansion before the peak of the pulse, the scale length increases in time with a rate of approximately 0.3 μm/ps, which is in agreement with the simple estimate of the sound velocity given above. In particular, the scale length at the peak of the pulse is predicted to be 4.1 μm, which is consistent with the measured value of $L = 4.3 \pm 1.2$ μm. However, after the peak of the pulse, a rapid increase in the density scale length is predicted by the 1-D simulation, the rate being now 1 μm/ps, that is, almost three times larger.

A comparison between the experiment, which provides a time-integrated measurement of the density scale length, and the prediction of hydrodynamic simulations, requires that a time-averaged value of the calculated scale length is obtained. A possible approach is to calculate the average scale length using the intensity of the laser pulse as a weighting function. A fifth-order polynomial fit of the curve of figure 3 was computed and the weighted average scalelength, $\bar{L}$ was calculated according to the definition

$$\bar{L} = \int_{-\Delta t}^{\Delta t} L(t) I_N(t)\, dt, \tag{1}$$

where I_N is the Gaussian laser intensity normalized according to $\int_{-\infty}^{+\infty} I_N(t)\, dt = 1$, and Δt is large compared to the full-width half-maximum (FWHM) of the laser pulse. This calculation gives an average scale length $\bar{L} = 5.5$ μm. Although this value is still consistent

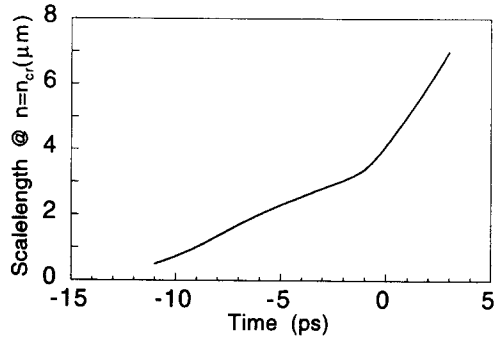

FIGURE 3. Electron density scale length at the critical density as a function of the time with respect to the peak of the 12-ps laser pulse as calculated by MEDUSA. The 268-nm laser pulse-shape was assumed to be Gaussian and the intensity on the solid Al target was 5×10^{16} W/cm^2.

with the one calculated from resonance absorption measurements, once the error is taken into account, nevertheless it suggests that the simulation overestimates the scale length. This effect is expected to be particularly important after the peak of the pulse, when the longitudinal density scale length becomes comparable with the transverse scale length, that is, of the order of the focal spot radius, that is, ≈ 10 μm. In these circumstances two-dimensional (2-D) effects start to contribute to the hydrodynamic expansion of the plasma. Simple thermodynamic considerations lead to the conclusion that the 1-D calculation is likely to overestimate the electron temperature in the subcritical region and the longitudinal density scale length.

On the other hand, the electron temperature in the underdense region strongly affects the collisional absorption because the inverse bremsstrahlung absorption coefficient depends upon $T_e^{-3/2}$, once the weak dependence of the Coulomb logarithm upon the electron temperature is neglected. This effect can have important consequences on the analysis of absorption of *S*-polarized data as discussed in the following section.

4.2. *Modelling of* S*-polarized absorption data*

Further insight into the condition of the plasma in the subcritical region can be gained from the analysis of the angular dependence of the *S*-polarized absorption data of figure 2. Some resonance absorption can take place in this case due to the spreading of angle of incidence in the *f*/4.7 focusing optics. However, we notice that with the measured value of the scale length, our plasma is entirely confined in the depth of focus of the laser that is ± 50 μm. In this region the laser beam wave front is approximately flat and the incident light can be considered a plane wave over the whole longitudinal plasma extent. Some residual spreading can still arise from laser beam nonuniformities, which can result in a local distortion of the wavefront. However, such contributions are expected to be effective only at small angles of incidence, typically of the order of the angular aperture of the focusing optics. Therefore, absorption of *S*-polarized light for $\theta \leq 6$ deg should be mostly accounted for by collisional absorption.

The expected contribution of collisional absorption has been evaluated assuming propagation of the laser beam in a stratified plasma with an exponential density profile (Kruer 1988). Refraction effects on the laser light reflected at the turning point and propagating backwards down the density gradient have been neglected in this analysis. In fact, there is experimental evidence that most of the laser light not absorbed by the target was scattered in an approximately *f*/1.5 cone. The fractional scattering calculated for a scale length of 4 μm was found to be in good agreement with the experimental data of figure 2 for an electron temperature of 5 keV. This value of the electron temperature is not far from the value predicted by numerical simulations, although in this case the comparison is limited to the normal incidence case. In fact, according to the simulations, the electron temperature is uniform over the subcritical region, its value being approximately 6 keV. However, in view of the conclusions formulated above on the validity of the 1-D simulation, in this case the apparent consistency between experiment and calculations could be only fortuitous and the result of simulations must be carefully examined.

An important aspect of the regime under investigation is that, at the irradiances typical of this experiment, the electron quiver velocity is comparable to the electron thermal velocity. At the laser intensity of 5×10^{16} W/cm^2, the ratio between the quiver and the thermal velocity is 0.44 in the case of a 2-keV plasma and becomes 0.62 for a 1-keV plasma. In addition, the swelling (Kruer 1988) of the laser field in the plasma density gradient can give up to a threefold increase of this parameter. Therefore, in the proximity of the criti-

cal layer, the quiver velocity can become higher than the local thermal velocity and consequently lead to a transition of the inverse bremsstrahlung absorption to a nonlinear regime.

The contribution of nonlinear effects in the collisional absorption of *S*-polarized light has been evaluated assuming propagation in an exponential density profile, considering an intensity dependent absorption coefficient and including swelling of the *E*-field in the density gradient. According to the conclusion reached above on the electron temperature in the subcritical region, an indicative temperature of 2 keV was assumed in the calculation. Two nonlinear mechanisms, namely the Langdon effect (Langdon 1980) and the standard nonlinear effect have been analyzed separately. The results of this calculation are summarized in table 1 for the case of normal incidence, and for different values of the incident intensity ranging from 10^{13} W/cm^2 to 10^{17} W/cm^2. The intensity at the turning point, and at the output of the 4-μm density scale length plasma, after reflection, is given as a fraction of the incident intensity, expressed in units of 10^{17} W/cm^2.

In the limit of low intensity, reported in the upper row of the table, nonlinear effects are expected to be negligible and in fact the calculation is in agreement with the value given assuming linear absorption only. At an intensity of 5×10^{16} W/cm^2 (third row from the top), that is, in the conditions of the absorption experiment described above, the calculation shows a strong reduction of the absorption due to nonlinear effects. In particular, the standard nonlinear effect, by itself, reduces the absorption efficiency from the 73% of the linear case to 27%. This value is in agreement with the measured value given in figure 2. In this case, the calculation was performed for different angles of incidence to make a direct comparison with the experimental data. The results are summarized by the solid line of figure 2. In addition, the dashed curve in the same graph shows the result obtained using the same condition but with no swelling effect included in the calculation.

The striking agreement between the experimental data and the results of this simple model suggests that, in the interaction conditions investigated here, nonlinear effects in the collisional absorption of laser light can play an important role. On the other hand, it is important to point out that the extent to which these effects influence the interaction is basically determined by the electron temperature in the laser–plasma interaction region. Nevertheless, the conclusions obtained here are basically independent from the particular choice of the electron temperature. In fact, for higher values of the electron temperature the *E*-field strength coefficient becomes smaller and the effective temperature, introduced in the linear absorption coefficient to account for nonlinear effects, approaches the thermal value. In particular, in the case of the 1-D model, the predicted electron temperature is high enough that nonlinear effects can be neglected. At this stage of the investigation, the balance

TABLE 1. Absorption of a 268-nm laser light after propagation and reflection in a 2-keV planar inhomogeneous plasma with a linear density profile of 4-μm scalelength. The incident intensity in the first column on the left is in units of 10^{17} W/cm^2, while the absorption coefficient in the last two columns on the right is given in percentage of the incident intensity.

I_{in}	I_{cr}^{Lang}	I_{cr}^{snl}	I_{out}^{Lang}	I_{out}^{snl}	A_L (%)	A_{snl} (%)
1.0E−4	5.1E−5	5.1E−5	2.9E−5	2.7E−4	71	73
0.1	0.07	0.067	0.05	0.044	50	56
0.5	0.36	0.43	0.27	0.37	46	27
1.0	0.73	0.93	0.55	0.86	45	14

between thermal and nonlinear effects in the absorption process is still undefined. However, an effective temperature in the laser–plasma interaction region of approximately 5 keV allows the whole set of absorption measurements presented here to be satisfactorily modelled. The role of absorption measurements in the transport of energy in the cold target will be discussed in the following section.

4.3. *Mass ablation rate*

The hydro-code MEDUSA was also used to calculate mass ablation rates. In the simulations, a 12-ps (FWHM) Gaussian laser pulse was incident onto a three-layer planar target at irradiances up to 3×10^{16} W/cm^2. The target consisted of a 10-μm-thick Mylar substrate coated with 2000 Å Al and overcoated with a thin (1000 Å) plastic (C–H) layer. The propagation, in the Lagrangian reference frame, of an isotherm of the heat front at a given temperature, is used to evaluate the mass-ablation rate from the results of the simulations. The mass-ablation rate was determined according to its definition, $\dot{m} = \rho \Delta r / \Delta t$, where ρ is the solid density of the ablated material, Δr is the burn-through depth, Δt is the time needed by the burn-through to take place. Figure 4 shows the calculated temporal evolution of electron temperature in the C–H and Mylar layers for an incident laser intensity of 3×10^{16} W/cm^2. The temperature in the C–H layer rises to several hundred eV in approximately 1 ps. After having ablated the middle layer (Al), the heat front reaches the Mylar substrate. The electron temperature in the Mylar substrate, at the first 10 cells allocated to this layer in the Lagrangian reference frame, is plotted in figure 4. A minimum delay $\Delta t \cong 9$ ps is predicted by the code between the time at which the C–H layer is heated at 400 eV and the time at which the first cell of the Mylar substrate reaches the same temperature. We observe that the dependence of such a delay upon the particular value of temperature chosen in the range taken into account was found to be very weak. This is consistent with the steepness of the heat front predicted by the classical theory of heat propagation.

From the plot of figure 4, one can immediately derive mass ablation rates by measuring the time interval, Δt for a given set of input parameters including laser intensity, heat flux limiter, and resonance absorption factor. The effect of resonance absorption on such results was examined in the simulations by varying the amount of laser energy damped at the crit-

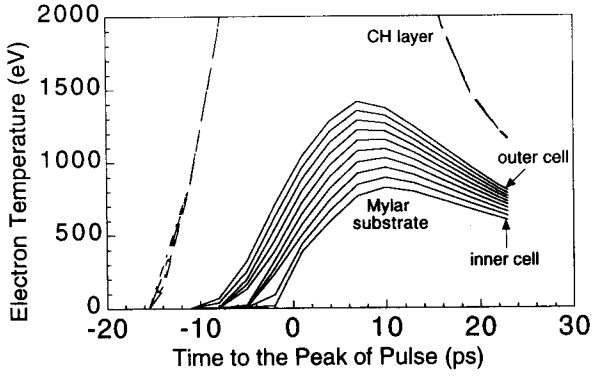

FIGURE 4. Temporal evolution of electron temperature in the C–H and Mylar layers as calculated by MEDUSA for an incident laser intensity of 3×10^{16} W/cm^2. Each curve gives the temperature of a given cell allocated by the Lagrangian reference frame to the C–H (dashed line) and to the Mylar substrate (solid line).

ical layer. It was found that fluctuations of the absorbed laser energy due to resonance absorption, within the range of 20% specified above, would produce variations of mass ablation rate within the experimental error of the XUV time-resolved spectra.

Finally, the calculated dependence of mass ablation rates upon the absorbed laser irradiance for two values of the flux limiter, that is, $f_L = 0.1$ and $f_L = 0.04$, was investigated and the result is displayed in figure 5. Ablation rates were calculated for several values of the incident intensity as indicated by the data points shown in the graph. The solid line was obtained from a linear fit of the numerical data. This plot clearly shows that the flux limiter plays an important role in these interaction conditions. In fact, according to the simulations, the mass ablation rate increases by 25% when the flux limiter is changed from 0.04 to 0.1. As a consequence of this increased flow of thermal energy toward the higher density region, the subcritical plasma, where absorption occurs, becomes cooler and more collisional and the absorption increases by approximately 20%. This dependence upon the flux-limiter is a strong indication of the fact that the classical theory of heat conductivity cannot properly describe this regime of interaction. In fact, as expected, the flux limiter starts playing a role when the temperature gradients are smaller than the electron mean-free path. An upper limit to the heat flux is therefore imposed using this phenomenological parameter. As shown by figure 5, the effect of this limitation increases with laser intensity as larger temperature gradients are established in the plasma.

The measured values of the mass ablation rate given above for the incident intensities of 3×10^{16} W/cm^2 and 4.3×10^{15} W/cm^2 are also plotted in figure 5. The incident intensity was converted into absorbed intensity according to the measured absorption as a function of the incident laser intensity (Riley *et al.* 1992). The mass ablation rate measured at the lower intensity is consistent with the calculated one for a flux limiter of 0.04. This value, though not very different, is smaller than that inferred by the 2-D FP simulation considered above. In that study it was found that the heat flux in the supercritical region was consistent with classical theory using a flux limiter of 0.1. However, we cannot exclude that other sources of error could make this experimental result consistent with the 2-D FP simulation. Further, in presence of efficient hot electron generation, as that arising from resonance absorption, transport processes can be strongly affected as a consequence of the increased electron mean-free path.

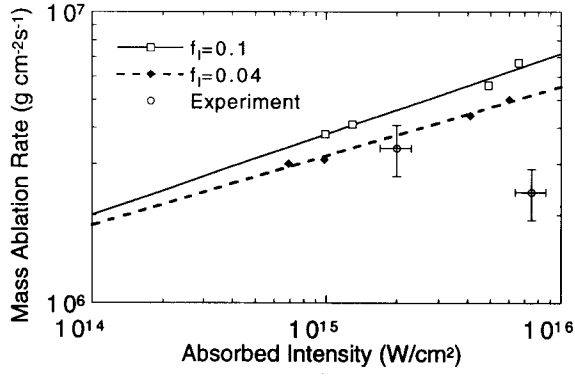

FIGURE 5. Mass ablation rate as a function of absorbed laser intensity, calculated by MEDUSA for two different values of the flux limiter. A layered (C-H-Al-Mylar) target was irradiated with a 12-ps Gaussian pulse and the average ablation rate of the middle Al layer is reported here. The result of the experimental measurement is also plotted in the same graph for comparison.

In contrast, a large discrepancy is found in the higher intensity regime, where the measured ablation rate is less than half of the calculated one. This would indicate a strong reduction of the heat flux compared with the lower intensity case. It is clear that this discrepancy cannot be simply explained in terms of the classical heat transport theory, as this conclusion would lead to an unacceptable value of the heat flux, orders of magnitude smaller than the free-streaming value. Several effects can be invoked to explain this discrepancy as discussed below.

5. Discussion

It has been pointed out (Bell 1994) that a complete modelling of the interaction regimes like that considered in this work would require a self-consistent treatment of nonlocal heat transport and magnetic field generation in a 2-D geometry. Nevertheless, in particular circumstances, one of these aspects can be dominant over the others and can therefore be dealt with independently. Self-generated magnetic fields and lateral heat propagation are are two of the most important processes that are distinctive of the 2-D behavior of the interaction process and that are not included in a 1-D modelling.

From the point of view of the ablation process, any lateral heat flow would result in less thermal energy being transported into the inner layers of the target, thus reducing the mass ablation rate. In a recent experiment (Al-Hadithi *et al.* 1994), lateral energy transport in plasmas produced by KrF laser pulses focused in a line has been investigated by studying X-ray emission from a tracer layer buried in a layered target. According to this study, regardless of the particular geometry, spot or line focus, adopted in the experiment, the key parameter to evaluate the importance of lateral transport is the ratio between the focal-spot width and the distance between the critical-density layer and the ablation surface.

On the other hand, the role played by lateral transport in the interaction of 3.5 ps, KrF laser pulses with solid Al targets, has also been investigated by using 2-D FP numerical simulations (Rickard *et al.* 1989). According to this study, even for relatively small values of the parameter introduced above, lateral transport is expected to involve only a small fraction of the total energy absorbed by the plasma. In fact, most of this energy is found to be efficiently transported axially in the cold target, even in the case of a focal spot as small as 20 μm, as in our case. Although this picture may not be strictly applicable to our case, due to the longer pulse length used in our experiment, it suggests that, in particular circumstances, mechanisms other than lateral transport must also be taken into account.

Strong self-generated magnetic fields (Haines 1986) can lead to a substantial inhibition of the thermal transport if the Larmor radius of the streaming electrons is small compared to their mean-free path. Indeed, strong self-generated magnetic fields can arise in the laser–plasma interaction region when the condition $\nabla n_e \times \nabla T_e \neq 0$ is fulfilled, ∇n_e and ∇T_e being the electron density gradient and electron temperature gradient, respectively. In the case of laser interaction with solid plane targets, such a condition can be easily verified near the edge of the laser focal spot (Stamper 1975). In this case the radial temperature gradient and the longitudinal density gradient give rise to a toroidal magnetic field around the focal spot whose temporal growth can be estimated according to the following expression (Stamper 1991)

$$\frac{\partial B}{\partial t} = \nabla \times \left(\frac{\nabla P}{n_e e}\right) = -\frac{1}{n_e e} \nabla n_e \times \nabla T_e, \tag{2}$$

where P is the plasma pressure, n_e is the electron temperature, and T_e is the electron temperature in energy units. In terms of the experimental parameters, namely the longitudi-

nal density scalelength L_{n_e} and the transverse temperature scalelength L_{T_e}, one can verify that

$$B \sim 9 t_{ps} T_{e,keV} L^{-1}_{T_e,\mu m} L^{-1}_{n_e,\mu m} \text{ MG}. \tag{3}$$

In our experimental conditions the pulse duration of 12 ps and the focal spot of 25 μm suggest a time scale $t \sim 10$ ps and $L_{T_e} \sim 10$ μm, respectively. Further, according to the experimental results given above we can assume an effective electron temperature in the critical region of 4 keV and a longitudinal density scalelength $L_{n_e} \sim 4$ μm. By inserting these values in equation (3) we find a magnetic field strength of $\sim$10 MG.

Indeed, experimental observations suggest that magnetic fields may be generated in our experimental conditions. Figure 6 shows an X-ray image of the laser–plasma interaction region obtained in the same interaction conditions described above but at a slightly higher irradiance of $\approx 10^{17}$ W/cm^2. The X-ray emitting region shown in figure 6 consists of an intense central region, approximately 25 μm in diameter, that is, equal to the FWHM of the laser focal spot. This central region is surrounded by a $\approx$30-μm-wide halo similar to that observed in previous experiments (Amiranoff 1982) with planar targets. The structure of X-ray images like the one shown in figure 6 was explained as due to the interaction of hot electrons with the cold material surrounding focal spot. In fact, in presence of electron plasma waves arising from resonance absorption, electrons can be accelerated and ejected down the density gradient, away from the target surface. Due to the presence of toroidal magnetic fields, these hot electrons are pulled back and hit the cold Al target around the focal spot, giving rise to K_α emission. The image of figure 6 was obtained by using an X-ray imaging device equipped with a 3-μm-thick Al foil as an X-ray filter to enhance the sensitivity of the system to K_α emission against other sources of radiation. In fact, Al plasma self-emission, mainly consisting of line emission from He-like and H-like Al ions is strongly attenuated by the K-shell absorption band of the Al filter. On the contrary, K_α emission is efficiently transmitted by the filter, its characteristic energy being smaller than the absorption edge energy of the filter.

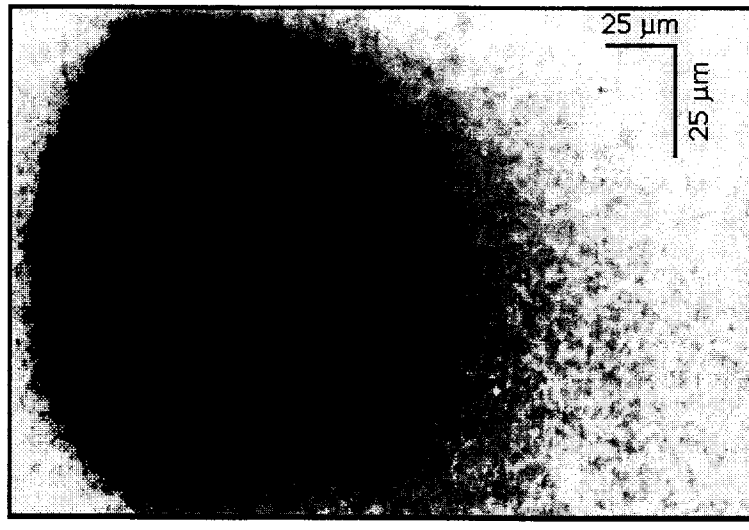

FIGURE 6. X-ray image of the interaction of a 12-ps laser pulse focused to a $\approx$25-μm focal spot on a solid Al target at an intensity of $\approx 10^{17}$ W/cm^2.

The importance of magnetic fields in thermal transport processes can be estimated by comparing the Larmor angular frequency of the streaming electrons, ω with the electron collision frequency, $1/\tau$, τ being the electron collision time. In terms of plasma parameters this condition can be written as (Bell 1994)

$$\omega\tau \sim 1.8 \times 10^2 \frac{T_{E,keV}^{5/2} \ln \Lambda t_{ps}}{Z n_{e,10^{22}\,\mathrm{cm}^{-3}} L_{T_e,\mu m} L_{n_e \mu m}} > 1. \tag{4}$$

For the experimental conditions considered above and assuming a fully ionized Al plasma and an electron density $n_e \sim 10^{22}$ cm^{-3} one finds that $\omega\tau \sim 10$. In other words, in the experimental conditions studied here, thermal transport could be heavily affected by magnetic fields. The effect of magnetic fields on the thermal conductivity, in the limit of large fields ($\omega\tau \gg 1$), has been studied by Braginskii (1965) and can be summarized by the expression of the heat flux

$$\mathbf{q} = -\kappa_{\parallel} \nabla_{\parallel} T_e - \kappa_{\perp} \nabla_{\perp} T_e - \kappa_{\wedge} \mathbf{b} \times \nabla_{\perp} T_e, \tag{5}$$

where the first and the second term describe, respectively, the components of the heat flux parallel and perpendicular to the magnetic field. The last term describes the heat flux perpendicular to both the component of the temperature gradient perpendicular to the magnetic field and the magnetic field itself, **b** being the unit vector parallel to the magnetic field. Taking into account the typical geometry of the laser–target interaction experiments, the heat flux in the longitudinal direction, that is, toward the target, is described by the second term of equation (5). According to the plasma conditions given above, the ratio of the longitudinal conductivity to the Spitzer conductivity is approximately 0.008. Such a flux limitation, compared to the values given by the 1-D simulation, supports the assumption that self-generated magnetic fields could strongly affect heat transport processes. In fact, these fields could account for an effective flux inhibition much greater than that suggested by previous experiments. It is clear, however, that a complete modelling of interaction regimes like that investigated here requires a self-consistent treatment of nonlocal heat transport and magnetic-field generation in a 2-D geometry.

6. Conclusion

The propagation of the heat wave in the interaction of picosecond laser pulses with solid targets was measured and correlated with absorption measurements of *S*- and *P*-polarized light. The mass-ablation rate for incident laser intensities greater than 10^{15} W/cm^2 was found to be smaller than that calculated by using a classical description of thermal transport. In particular, at incident intensities greater than 10^{16} W/cm^2, the measured mass-ablation rate was found to be less than 50% of the calculated one. These results indicate that some other processes occur during the interaction, resulting in a dramatic reduction of the longitudinal heat flux. The occurrence of self-generated magnetic fields, supported by indirect experimental observations, is taken into account as a possible explanation of the observed flux inhibition. According to the measured electron temperature and density scale lengths, a magnetic field of the order of 10 MG is expected in the experimental conditions considered here. Following the theory of magnetized transport, this field provides, by itself, a semiquantitative explanation of the experimental results on thermal transport reported in this paper.

REFERENCES

AL-HADITHI, Y. *et al.* 1994 *Phys. Plasmas* **1**, 1279.

AMIRANOFF, F. *et al.* 1982 *J. Phys. D: Appl. Phys.* **15**, 2463.

BELL, A.R. 1994 *Transport in laser produced plasmas* (SUSSP, St. Andrews).
BRAGINSKII, S.I. 1965 *Reviews of Plasma Physics*, Vol. 1, (Consultants Bureau, New York) p. 205.
CHRISTIANSEN, J.P. *et al.* 1974 *Comp. Phys. Comm.* **7**, 271.
DAHMANI, F. & KERDJA, T. 1991 *Phys. Rev.* A **44**, 2649.
GIZZI, L.A. 1994 Ph.D. Thesis (Imperial College of Science, Technology and Medicine, London).
GODWIN, P. *et al.* 1977 *Phys. Rev. Lett.* **39**, 1198.
HAINES, M.G. 1986 *Can. J. Phys.* **64**, 912.
JAANIMAGI, A. 1986 *Phys. Rev. A* **34**, 1322.
KEY, M.H. *et al.* 1983 *Phys. Fluids* **26**, 2011.
KRUER, W.L. 1988 *The Physics of Laser Plasma Interactions* (Addison-Wesley, New York).
LANGDON, B. 1980 *Phys. Rev. Lett.* **44**, 575.
MARTIN, A. & WIESE, W.L. 1983 *J. Chem. Ref. Data* **15**, 537.
MEYER-TER-VEHN, J. *et al.* 1984 *Phys. Lett.* **108**, 410.
MURNANE, M. & KAPTEYN, H.D. 1991 *Phys. Fluids* **3**, 2409.
NAKANO, N. *et al.* 1984 *Appl. Optics* **23**, 2386.
PERRY, A. *et al.* 1989 *Phys. Rev.* A **39**, 2565.
RICKARD, J. *et al.* 1989 *Phys. Rev. Lett.* **62**, 2687.
RILEY, D. *et al.* 1992 *Annual Report Rutherford Appleton Laboratory (UK)*, RAL-93-020, p. 16.
RILEY, D. *et al.* 1993 *Phys. Rev.* E **48**, 4855.
ROSEN, D. 1990 *Phys. Fluids* **2**, 1461.
SPITZER, L., JR. & HARM, R. 1953 *Phys. Rev.* **89**, 977.
STAMPER J.A. 1975 *Phys. Rev. Lett.* **34**, 138.
STAMPER J.A. 1991 *Laser Part. Beams* **9**, 841.